A Theoretical and Experimental Study of the Internal Circulation in Water Drops Falling at Terminal Velocity in Air

B. P. LECLAIR[1] AND A. E. HAMIELEC

Dept. of Chemical Engineering, McMaster University, Hamilton, Ontario, Canada

AND H. R. PRUPPACHER AND W. D. HALL

Dept. of Meteorology, University of California, Los Angeles 90024

(Manuscript received 8 October 1971, in revised form 10 January 1972)

ABSTRACT

Four theoretical approaches are presented for quantitatively determining the intensity of the internal circulation and the flow patterns inside and outside liquid water spheres falling at terminal velocity in air. The first approach assumes creeping flow outside and inside a water sphere, the second assumes potential flow outside and inviscid motion inside a water sphere, the third makes use of boundary layer theory, and the fourth approach uses a numerical method to solve the full Navier-Stokes equation of motion inside and outside a water sphere. The theoretical predictions are compared with data obtained from new quantitative wind tunnel experiments on spherical and deformed water drops. The results show that the creeping flow analysis greatly underestimates the strength of the internal velocity while the inviscid flow analysis greatly overestimates it. On the other hand, the results of the boundary layer approach and of the numerical approach agree reasonably well with the experimental data for drops with radii $<500\,\mu$. For larger drops the results of the boundary layer approach greatly overestimate the strength of the internal circulation and predict a completely wrong trend of the variation of the internal velocity with drop size, while the numerical results, although somewhat overestimating the circulation strength, predict the trend correctly. Reasonably good agreement is also found between the observed flow patterns inside the drop and those numerically predicted. In two appendices the effect of the internal circulation on drop shape and hydrodynamic drag is discussed.

1. Introduction

Despite the large amount of experimental and theoretical work that has been reported in the literature on internal circulation in liquid drops falling in other liquids and in gas bubbles rising in liquids, little progress has been made since the fundamental paper of McDonald (1954) in understanding the mode of internal circulation in liquid drops falling in a gas. The presence of a vortex in water drops falling in air was suspected by Lenard (1904), Blanchard (1949) and Kinzer and Gunn (unpublished), and has been verified by the wind tunnel studies of Pruppacher and Beard (1970) for small drops and those of Garner and Lane (1959) for large drops.

In this paper four theoretical approaches will be presented for quantitatively predicting the strength of the internal circulation and the flow patterns inside and outside a liquid water sphere in air. The results of this investigation are then compared with new, quantitative wind tunnel data on spherical and deformed water drops.

[1] Present affiliation: Canada Centre for Inland Waters, Burlington, Ontario.

2. Experiment

The experimental study of the internal circulation inside water drops falling at terminal velocity in air was carried out with a wind tunnel method similar to the one described in detail by Pruppacher and Beard. In order to allow a drop to come into equilibrium with the environment the drop was freely suspended in the air stream for about 1 min before measurements were made. The motion inside a drop, visualized by carbon or aluminum particles, was qualitatively investigated by a 16-mm motion picture film using 64 frames per second, and quantitatively recorded by a method involving streak photography. From a knowledge of the apparent streak length, the refractive index of water and air, and the drop shape found by the method of Pruppacher and Pitter (1971), the true lengths of the particle trajectories inside a drop were determined following a method discussed in detail by Kintner *et al.* (1961) and Horton *et al.* (1965). This method involves correcting the apparent travel distance of a particle, which is larger than the actual travel distance as a result of magnification by the drop acting as a lens, by means of well-known relations of geometrical optics. From a knowledge of the true trajectory lengths and the shutter

speed (typically 1/250 to 1/500 sec) of an accurately calibrated Nikon-F camera, the velocities of the particles in the meridian plane of the drop parallel to the plane of the film were computed. In total, 226 streaks were measured from 111 drops ranging in radius between 310 μ and 1.68 mm. The streaks analyzed extended between $\theta \approx 50°$ and $\theta \approx 100°$, where θ is the angle measured from the foreward stagnation point of the drop. The internal velocities derived from these streaks were assumed to represent average surface velocities between those angles. The velocities thus derived varied appreciably, particularly within the larger drops. This is indicated by the error bars in Fig. 1 where the internal velocity, v_i $(a,75°)$, at the drop's surface and at $\theta = 75°$, is plotted as a function of the equivalent drop radius a_0 (which is the radius of a sphere that has the same volume as the deformed drop in question). In addition to the present experimental values, the experimental values of Garner and Lane (1959) for drops that were suspended in the air during times > 15 sec are also entered in Fig. 1. For unclear reasons Garner and Lane applied a standard correction of 1/3 to the particle trajectory in a drop independent of drop size. This is clearly incorrect since the magnification of a particle trajectory in a drop is a function of drop shape and thus of drop size. We therefore re-analyzed the Garner and Lane values in the light of the Kinter and Horton correction method and used those corrected values as a lower bound. As an upper bound we chose to use the uncorrected values which apply to particles whose trajectories were close to the drop surface. Curve 4 in Fig. 1 connects the maximum values of all the experimental internal velocities. We made the assumption that these maximum values represent reasonably close approximations to $v_i(a,75°)$,

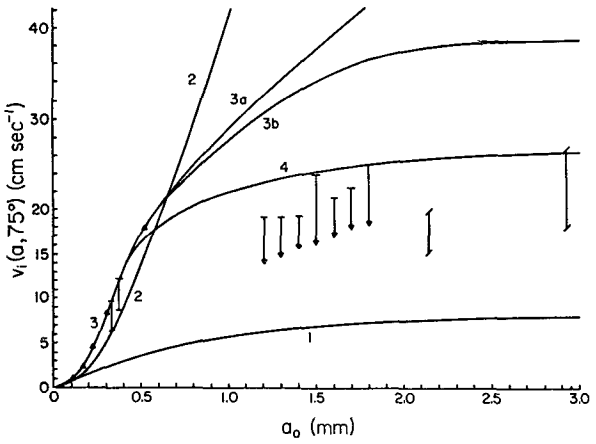

FIG. 1. Comparison between experimentally and theoretically determined velocity at the surface of a circulating water drop in air: curve 1, Hadamard-Rybczynski theory for water sphere; curve 2, bouudary layer theory for water sphere; curve 3a and triangles, numerical approach for water sphere with terminal velocity of spherical drops; and curve 3b, numerical approach for water spheres with terminal velocity of deformable drops. Error bars with horizontal end are for present experimental results; those with inclined ends for experiments of Garner and Lane (1959). Curve 4 is the upper bound for experimental results.

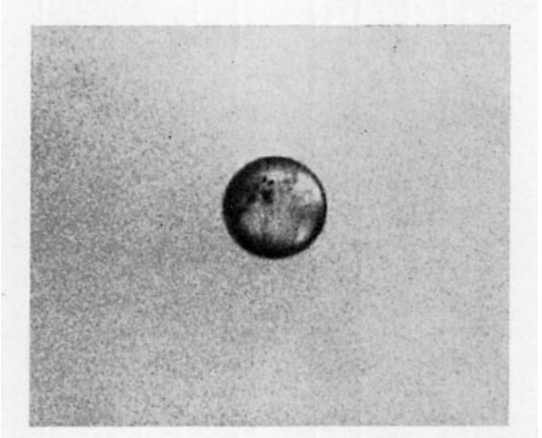

FIG. 2. Visualized flow pattern inside a water drop of 315 μ radius suspended at terminal velocity in the cloud tunnel.

and that they can be used for comparison with theoretically predicted internal velocities.

In order to display the flow pattern inside a water drop by means of a photograph which has suitable contrast after reproduction, we recorded the internal circulation by taking motion pictures inside drops which contained large numbers of tracer particles. In Fig. 2 the flow pattern inside a drop of radius 315 μ is reproduced from a frame of this motion picture.

3. Theory

a. Creeping flow analysis

In this approach a uniform, axisymmetric, very slow viscous flow past a liquid sphere shall be assumed. The basic hydrodynamics for this situation has been worked out by Hadamard (1911) and by Rybczinski (1911) and is summarized by Happel and Brenner (1965). According to these authors, streamfunctions ψ_0 and ψ_i of the flow outside and inside the water sphere can be written as

$$\psi_0 = \tfrac{1}{4} U_\infty \sin^2\theta \left[-3ar\left(\frac{1+\frac{2}{3}\sigma}{1+\sigma}\right) + 2r^2 + \frac{a^3}{r}\left(\frac{1}{1+\sigma}\right)\right], \quad (1)$$

$$\psi_i = \tfrac{1}{4} U_\infty \sin^2\theta \left(\frac{\sigma}{1+\sigma}\right) r^2 \left(\frac{r^2}{a^2} - 1\right), \quad (2)$$

where r is the radial distance from the sphere center, a the sphere radius, U_∞ the velocity of the fluid far away from the sphere, $\sigma = \mu_0/\mu_i$, and μ_0 and μ_i are the dynamic viscosities outside and inside of the sphere. From Eq. (2) the tangential velocity $v_i(r,\theta)$ at an arbitrary position r, θ inside the drop can then be found, i.e.,

$$v_i(r,\theta) = v_i = \frac{1}{r\sin\theta}\left(\frac{\partial \psi_i}{\partial r}\right)_\theta = \frac{\sin\theta}{2}\left(\frac{\sigma}{1+\sigma}\right)\frac{U_\infty}{a^2}(2r^2 - a^2). \quad (3)$$

Since $r = a$ at the surface of the sphere, we have

$$v_i(a,\theta) = \frac{\sin\theta}{2}\left(\frac{\sigma}{1+\sigma}\right) U_\infty. \quad (4)$$

For a water sphere in air, $\mu_0 \ll \mu_i$, and Eq. (4) becomes

$$v_i(a,\theta) = -\frac{1}{2}\frac{\mu_0}{\mu_i} U_\infty \sin\theta. \tag{5}$$

Eq. (5) was evaluated for $\mu_i = \mu_{\text{water}} = 1.0019 \times 10^{-2}$ poise, $\mu_0 = \mu_{\text{air}} = 1.818 \times 10^{-4}$ poise, and $\theta = 75°$. For U_∞ values for the terminal fall velocities determined by Beard and Pruppacher (1969) and by Gunn and Kinzer (1949) were used. The results of this computation are plotted in Fig. 1 as curve 1. An evaluation of ψ_0 and ψ_i shows readily that the flow fields outside and inside the water sphere are symmetric with respect to planes perpendicular and parallel, respectively, to the flow axis of the flow outside the drop. Inside the drop the velocity of the liquid is zero along a stagnation ring where $\theta = \pi/2$ and where $r = a/2^{\frac{1}{2}}$.

b. Inviscid flow analysis

For this approach it is assumed that the flow inside the water sphere can be represented by an inviscid axisymmetric vortex which, according to Milne-Thomson (1967), has the streamfunction

$$\psi_i = -\frac{A}{10}(a^2 - r^2) r^2 \sin^2\theta. \tag{6}$$

Outside the sphere we shall assume potential flow with the streamfunction

$$\psi_0 = -\tfrac{1}{2} U_\infty r^2 \sin^2\theta \left(1 - \frac{a^3}{r^3}\right). \tag{7}$$

Through the boundary condition $\partial\psi_0/\partial r = \partial\psi_i/\partial r$ at $r = a$, the constant A becomes $15U_\infty/(2a^2)$; therefore,

$$\psi_i = -\frac{3U_\infty}{4a^2}(a^2 - r^2) r^2 \sin^2\theta. \tag{8}$$

This streamfunction describes what is known as Hill's spherical vortex. For the internal velocity we find from Eq. (8) that

$$v_i = \frac{3U_\infty}{2a^2}(2r^2 - a^2) \sin\theta, \tag{9}$$

which for $r = a$ becomes

$$v_i(a,\theta) = \tfrac{3}{2} U_\infty \sin\theta. \tag{10}$$

The flow fields outside and inside the water sphere are symmetric, and the flow inside has, as in the case of creeping flow, a stagnation ring at $\theta = \pm\pi/2$ and $r = a/2^{\frac{1}{2}}$. This result is expected as the streamfunctions given by Eqs. (2) and (6) are identical except for the pre-factors.

c. Boundary layer analysis

McDonald (1954) first suggested that for a more realistic theory of the internal circulation of a water drop in air the presence of a hydrodynamic boundary layer between the drop surface and the external flow should be recognized. Unfortunately, in his analysis McDonald made two questionable assumptions which will be pointed out below. In presenting an improved version of McDonald's theory we shall again assume uniform axisymmetric flow past a liquid sphere inside of which the flow can be represented by an inviscid axisymmetric vortex. The streamfunction inside the sphere is then given by Eq. (6) and the internal velocity becomes

$$v_i = \frac{A}{5}(2r^2 - a^2) \sin\theta. \tag{11}$$

In terms of its derivative with respect to r, Eq. (11) may be written as

$$v_i = \frac{2r^2 - a^2}{4r}\left(\frac{\partial v_i}{\partial r}\right)_\theta, \tag{12}$$

or at $r = a$

$$v_i(a,\theta) = \tfrac{1}{4} a \left(\frac{\partial v_i}{\partial r}\right)_\theta. \tag{13}$$

Continuity of the tangential stress across the liquid sphere surface at $r = a$ requires (Happel and Brenner, p. 128) that

$$\mu_i \left[\frac{\partial}{\partial r}\left(\frac{1}{r^2}\frac{\partial \psi_i}{\partial r}\right)\right]_{a,\theta} = \mu_0 \left[\frac{\partial}{\partial r}\left(\frac{1}{r^2}\frac{\partial \psi_0}{\partial r}\right)\right]_{a,\theta}, \tag{14}$$

which can be rewritten as

$$\mu_i \left[\frac{\partial}{\partial r}\left(\frac{v_i}{r}\right)\right]_{a,\theta} = \mu_0 \left[\frac{\partial}{\partial r}\left(\frac{v_0}{r}\right)\right]_{a,\theta}, \tag{15}$$

where $v_0(r,\theta) = v_0$ is the tangential velocity at an arbitrary position r, θ outside the liquid sphere. Performing the differentiation in Eq. (15) we obtain

$$a\left(\frac{\partial v_i}{\partial r}\right)_a = v_i(a,\theta) + \frac{\mu_0}{\mu_i} a^2 \frac{\partial}{\partial r}\left(\frac{v_0}{r}\right), \tag{16}$$

in contrast to McDonald who approximated the differentiation and found that $a(\partial v_i/\partial r)_a = (\mu_0/\mu_i) a(\partial v_0/\partial r)_a$. After substituting (16) into (13), we find for the internal velocity

$$v_i(a,\theta) = \frac{1}{3}\frac{\mu_0}{\mu_i} a^2 \left[\frac{\partial}{\partial r}\left(\frac{v_0}{r}\right)\right]_a. \tag{17}$$

In order to evaluate $v_i(a,\theta)$ we have to determine $[\partial/\partial r(v_0/r)]_a$, which necessitates a knowledge of the velocity distribution outside the liquid sphere. For this reason we shall assume the existence of a boundary layer of thickness δ in the flow just outside the sphere. Using the results of Tomotika's (1937) boundary layer theory

for the point of zero static pressure gradient on the sphere, which for $10^3 \leqslant N_{Re} \leqslant 10^5$ lies at about $\theta = 75°$, we obtain

$$\left[\frac{\partial}{\partial r}\left(\frac{v_0}{r}\right)\right]_a = \frac{2v_0(\delta,75°)}{a\delta}, \tag{18}$$

where $v_0(\delta,75°)$ is the velocity at $\theta = 75°$ and at the outer edge of the boundary layer, $N_{Re} = 2aU_\infty/\nu$ is the Reynolds number, ν the kinematic viscosity of the external fluid, and δ, according to Tomotika, is given by $\delta = 3.8\nu N_{Re}^{\frac{1}{2}}/v_0(\delta,75°)$. In contrast, McDonald postulated the existence of a linear boundary layer and approximated $[\partial/\partial r(v_0/r)]_a \approx (1/a)(\partial v_0/\partial r)_a \approx v_0(\delta,\theta)/(a\delta)$. The new results lead to

$$v_i(a,75°) = \frac{2}{3}\frac{\mu_0}{\mu_i}\frac{v_0(\delta,75°)}{\delta/a}$$

$$= \frac{1}{11.4}\left(\frac{\mu_0}{\mu_i}\right)\frac{N_{Re}^{\frac{1}{2}}}{U_\infty}[v_0(\delta,75°)]^2. \tag{19}$$

Since $v_0(\delta,75°)$ is approximately proportional to U_∞,

$$v_i(a,75°) \propto N_{Re}^{\frac{1}{2}}. \tag{20}$$

Assuming potential flow outside the boundary layer we can find $v_0(\delta,75°)$, according to Tomotika, from $v_0(\delta,\theta) = (3/2)U_\infty \sin\theta$, or, more realistically from an experimental pressure distribution around a sphere and the relation

$$v_0(\delta,\theta)/U_\infty = \left[1 - \frac{p_\theta - p_\infty}{(\rho/2)U_\infty}\right]^{\frac{1}{2}},$$

which is easily derived from Bernoulli's Law.

More accurate values for $v_0(\delta,75°)/U_\infty$ can be obtained from velocity profiles outside a sphere using numerical solutions to the Navier Stokes equations of motion. We have obtained such solutions for circulating water spheres of various Reynolds numbers (see Section 3d). A plot of $v_0(r,75°)/U_\infty$ vs r/a is given in Fig. 3, where a comparison is also made with the velocity distribution outside a rigid sphere (see LeClair *et al.*, 1970 and Pruppacher *et al.*, 1970). It is seen from this figure that with increasing distance from the sphere surface $v_0(r,75°)/U_\infty$ increases at first, reaches a maximum, and then decreases again to approach sin 75° as r approaches infinity. The position of the peak value of $v_0(r,75°)/U_\infty$ can be considered to mark the edge of the boundary layer and thus represents $v_0(\delta,75°)$. One also notes from Fig. 3 that the boundary layer around a liquid sphere is slightly thinner than that on a rigid sphere of the same Reynolds number; the difference, however, is almost negligibly small for a water sphere in air. Inserting into Eq. (19) the numerically derived values for $v_0(\delta,75°)$, and using the experimental values of Beard and Pruppacher and Gunn and Kinzer for U_∞, values for $v_i(a,75°)$ were calculated and are shown in Fig. 1 as curve 2.

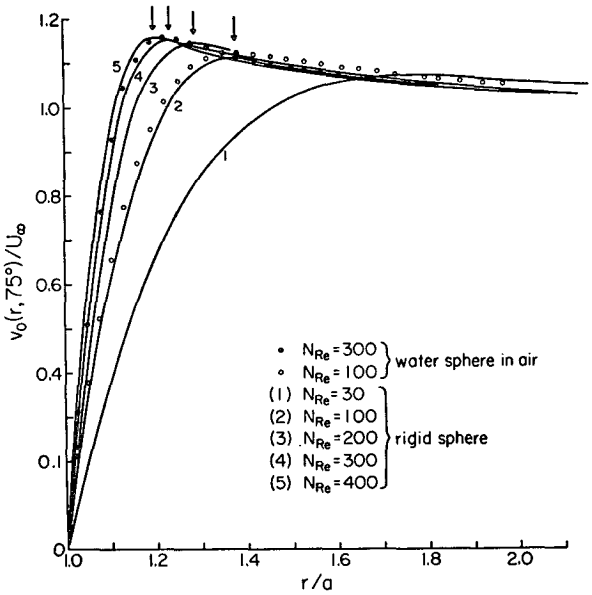

FIG. 3. Variation of the tangential velocity outside a circulating water sphere with distance from the sphere surface, computed by the numerical approach.

d. Numerical approach

LeClair *et al.* and Pruppacher *et al.* have recently reported on the results of their theoretical investigation of the flow past a rigid sphere using numerical methods. This investigation has now been extended to include flow past a liquid sphere; details are given by LeClair (1970). In this article only a brief summary of the work shall be given. Using the dimensionless variables $r' = r/a$, $\psi' = \psi/U_\infty a^2$, $\zeta' = \zeta a/U_\infty$, where ψ is the streamfunction and ζ the vorticity, and then dropping the primes for simplicity, the Navier-Stokes equations of motion for viscous, incompressible, axisymmetric flow can be written in spherical coordinates and in nondimensionalized forms as (LeClair *et al.*, 1970)

$$E^2\psi = \zeta r \sin\theta, \tag{21}$$

$$\frac{N_{Re}}{2}\left[\frac{\partial\psi}{\partial r}\frac{\partial}{\partial\theta}\left(\frac{\zeta}{v\sin\theta}\right) - \frac{\partial\psi}{\partial\theta}\frac{\partial}{\partial r}\left(\frac{\zeta}{r\sin\theta}\right)\right]\sin\theta$$

$$= E^2(\zeta r \sin\theta). \tag{22}$$

In the case of a fluid sphere these equations apply separately inside and outside the drop. An exponential step size in radial direction was used in the flow field outside the drop by the substitution $r = e^z$, and equal intervals in z were taken; inside the drop equal intervals of r were used. For these conditions the Navier-Stokes equations of motion can be written for the flow outside

TABLE 1. Variation of the nondimensionalized pressure at the surface of a liquid sphere, computed in the numerical analysis.

N_{Re}	θ (deg)							
	0	12	24	36	48	60	72	84
	96	108	120	132	144	156	168	180
30	1.3186	1.2349	1.0005	0.6599	0.2758	−0.0859	−0.3711	−0.5500
	−0.6212	−0.6072	−0.5417	−0.4563	−0.3726	−0.3032	−0.2365	−0.2398
100	1.1035	1.0170	0.7757	0.4292	0.0484	−0.2905	−0.5244	−0.6235
	−0.6015	−0.5080	−0.3899	−0.3130	−0.2545	−0.2105	−0.1708	−0.1525
300	1.0363	0.9419	0.6801	0.3098	−0.0852	−0.4147	−0.6055	−0.6295
	−0.5284	−0.3963	−0.3039	−0.2593	−0.2494	−0.2314	−0.1789	−0.1450

TABLE 2. Variation of the nondimensionalized vorticity at the surface of a liquid sphere, computed in the numerical analysis.

N_{Re}	θ (deg)							
	0	12	24	36	48	60	72	84
	96	108	120	132	144	156	168	180
30	0.0	1.6745	3.1569	4.2860	4.9464	5.0888	4.7426	4.0149
	3.0714	2.0956	1.2401	0.5923	0.1741	−0.0318	−0.0666	0.0
100	0.0	3.1681	5.9560	8.0349	9.1513	9.1705	8.1242	6.2561
	4.0250	1.9837	0.5303	−0.2733	−0.6568	×0.8262	−0.6314	0.0
300	0.0	5.7221	10.7138	14.3392	16.0918	15.6626	13.0408	8.7351
	4.0397	0.6445	−0.7794	−0.8742	−1.0690	−2.2816	−2.2232	0.0

the drop as

$$\frac{N_{Re}}{2}\left[\frac{\partial\psi_0}{\partial z}\frac{\partial}{\partial\theta}\left(\frac{\zeta_0}{e^z\sin\theta}\right)-\frac{\partial\psi_0}{\partial\theta}\frac{\partial}{\partial z}\left(\frac{\zeta_0}{e^z\sin\theta}\right)\right]e^z\sin\theta = e^{2z}E^2(\zeta_0 e^z\sin\theta), \quad (23)$$

$$\zeta_0 e^{3z}\sin\theta = e^{2z}E^2\psi_0, \quad (24)$$

and for inside the drop as

$$\left(\frac{\mu_0}{\mu_i}\right)\left(\frac{\rho_i}{\rho_0}\right)\frac{N_{Re}}{2}\left[\frac{\partial\psi_i}{\partial r}\frac{\partial}{\partial\theta}\left(\frac{\zeta_i}{r\sin\theta}\right)-\frac{\partial\psi_i}{\partial\theta}\frac{\partial}{\partial r}\left(\frac{\zeta_i}{r\sin\theta}\right)\right]\sin\theta = E^2(\zeta_i r\sin\theta), \quad (25)$$

$$\zeta_i r\sin\theta = E^2\psi_i. \quad (26)$$

These equations are constrained by the following boundary conditions: 1) far from the drop at $r=r_\infty$, $z=z_\infty$, where undisturbed parallel flow is assumed $\psi_0=\frac{1}{2}e^{2z_\infty}\sin^2\theta$, $\zeta_0=0$; 2) along the axis of symmetry $\theta=0$, π, we have $\psi_0=\zeta_0=\psi_i=\zeta_i=0$; 3) across the fluid-fluid interface there is no material transfer and thus $r=1$, $z=0$; $\psi_0=\psi_i=0$; and 4) to express continuity of tangential stress τ across the interface, we write $\tau_0(r,\theta)=\tau_i(r,\theta)$ from which, for $r=1$,

$$\partial^2\psi_0/\partial z^2-2\partial\psi_0/\partial z=(\mu_i/\mu_0)[(\partial^2\psi_i/\partial r^2)-(2\partial\psi_i/\partial r)].$$

Eqs. (23)–(26) together with the above boundary conditions were evaluated numerically for water spheres in air with $\mu_0/\mu_i=1.82\times10^{-2}$, $\rho_i/\rho_0=836.056$, and for Reynolds numbers of 10, 30, 57, 100, 300 and 400 [for details see LeClair (1970)]. From a knowledge of the streamfunction and vorticity fields the frontal stagnation pressure was obtained from the relation

$$k(a,\theta=0)=1+\frac{8}{N_{Re}}\int_1^{r_\infty}\left(\frac{\partial\zeta}{\partial\theta}\right)_{\theta=0}\frac{dr}{r}, \quad (27)$$

the surface pressure at an angle θ from

$$k(a,\theta)=k(a,\theta=0)+\frac{4}{N_{Re}}\int_0^{\theta}\left(\frac{\partial\zeta}{\partial r}+\zeta\right)_{r=1}d\theta-v^2, \quad (28)$$

and the internal velocity at the drop surface from

$$v_i(r=1,\theta)=\frac{1}{\sin\theta}\left(\frac{\partial\psi_i}{\partial r}\right)_{r=1}, \quad (29)$$

where $k(a,\theta)=p(a,\theta)-p_\infty/(\frac{1}{2}\rho U_\infty^2)$, and v is the tangential velocity of the flow field. Numerical values for τ, ζ and k are given in Tables 1–3 for $N_{Re}=10$, 30, 300. For the same Reynolds numbers the streamline and vorticity contours of the flow inside and outside the water sphere are given in Figs. 4–6 to which Table 4 is a key. In Table 5 the parameters which characterize the significant features of the flow inside and outside the water sphere are compiled for given Reynolds numbers and compared to the parameters of flow past a rigid sphere. As in the case of a rigid sphere, a standing eddy develops

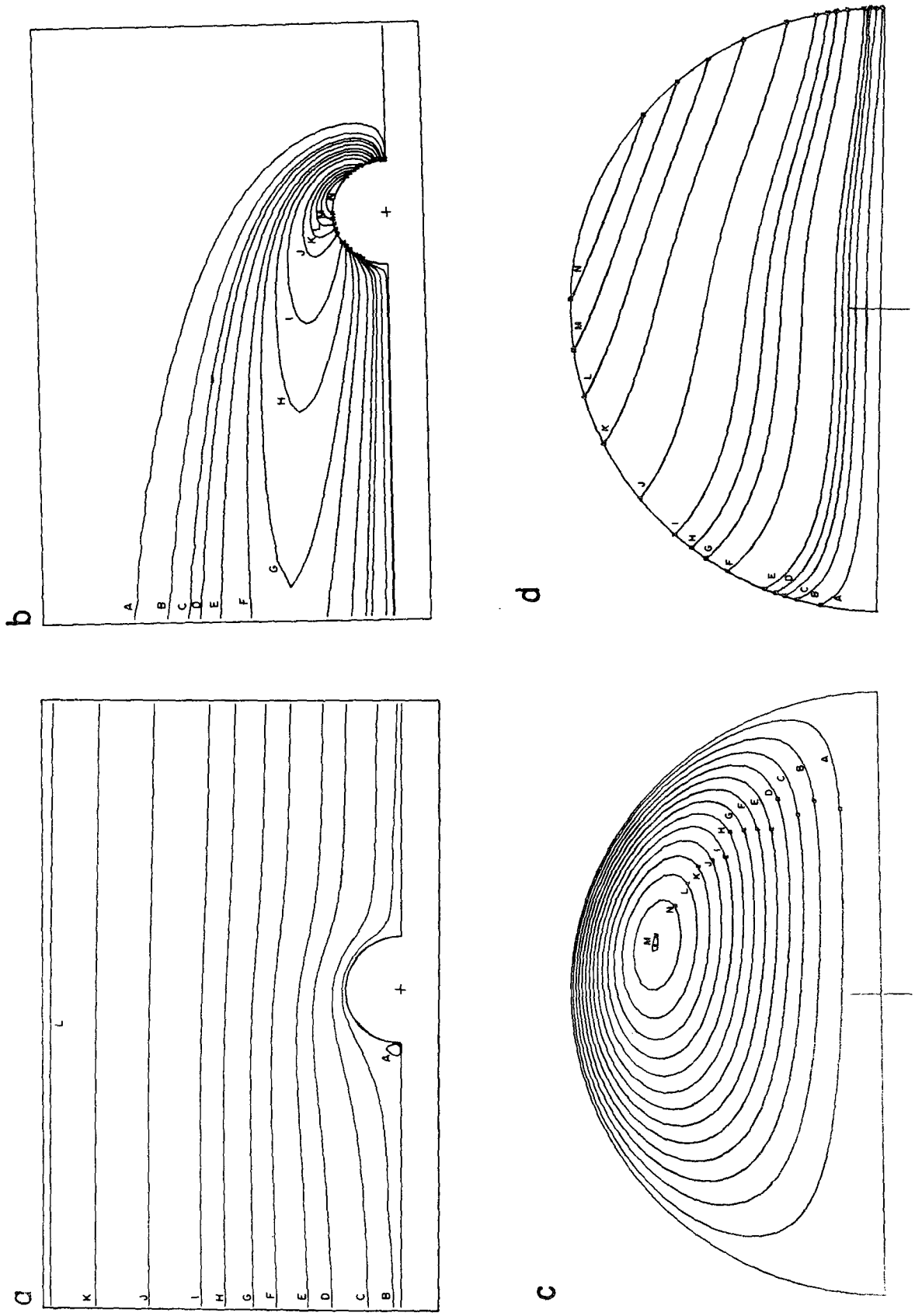

FIG. 4. Flow fields (a,c) and vorticity fields (b,d) outside and inside a circulating water sphere for $N_{Re}=30$ as computed by numerical approach.

TABLE 3. Variation of the nondimensionalized tangential stress at the surface of a liquid sphere, computed in the numerical analysis.

N_{Re}	θ (deg)							
	0	12	24	36	48	60	72	84
	96	108	120	132	144	156	168	180
30	0.0	1.6966	3.1949	4.3289	4.9800	5.0996	4.7225	3.9655
	3.0041	2.0268	1.1829	0.5524	0.1509	−0.0425	−0.0700	0.0
100	0.0	3.1939	6.0030	8.0943	9.2093	9.2103	8.1304	6.2229
	3.9640	1.9189	0.4805	−0.3055	−0.6763	−0.8324	−0.6293	0.0
300	0.0	5.7906	10.8824	14.6577	16.5525	16.2246	13.5712	9.0537
	4.0686	0.5351	−0.8638	−0.9225	−1.1146	−2.3021	−2.2235	0.0

TABLE 4. Numerical values of the streamline and vorticity contours shown in Figs. 4–6.

Contour	$N_{Re}=30.0$ Fig. no.				$N_{Re}=100.0$ Fig. no.				$N_{Re}=300.0$ Fig. no.			
	3a	3b	3c	3d	4a	4b	4c	4d	5a	5b	5c	5d
A	0.0	0.001	0.0001	0.0001	−0.008	−0.2	0.0001	−0.003	−0.035	−0.8	0.0	−0.015
B	0.01	0.01	0.00025	0.0003	−0.005	−0.1	0.0003	−0.001	−0.02	−0.6	0.0001	−0.01
C	0.1	0.03	0.0004	0.0005	−0.001	0.0	0.0007	−0.0002	−0.005	−0.4	0.0002	−0.005
D	0.5	0.05	0.00055	0.0007	0.0	0.01	0.001	0.0001	0.0	−0.2	0.0005	−0.001
E	1.0	0.1	0.0007	0.001	0.001	0.1	0.003	0.0006	0.002	0.0	0.001	−0.0001
F	2.0	0.2	0.00035	0.003	0.01	0.25	0.007	0.001	0.01	0.01	0.0015	0.0001
G	3.0	0.3	0.001	0.005	0.1	0.5	0.01	0.002	0.05	0.1	0.002	0.001
H	4.5	0.5	0.00115	0.007	0.5	1.0	0.013	0.006	0.1	0.5	0.0025	0.01
I	6.0	0.8	0.0013	0.01	1.0	2.0	0.017	0.01	0.5	1.0	0.003	0.05
J	10.0	1.5	0.00145	0.02	1.5	3.0	0.02	0.04	1.0	2.0	0.0035	0.1
K	15.0	2.0	0.0016	0.04	2.0	4.0	0.025	0.08	2.0	3.0	0.004	0.15
L	20.0	2.5	0.00175	0.06	2.5	5.0	0.030	0.12	—	5.0	0.0045	0.2
M	—	3.0	0.0019	0.08	3.0	6.0	0.035	0.16	—	8.0	0.0049	0.25
N	—	3.5	0.0020	0.1	—	7.0	0.038	0.20	—	11.0	—	0.3

TABLE 5. Comparison between the characteristics of the flow of air past a circulating and a rigid water sphere, computed in the numerical analysis.

N_{Re}	(L/d) Liquid circulating sphere	(L/d) Rigid sphere	r_{st}'	θ_{st}	$\theta_{(v_i)\max}$	$\theta_{\zeta\max}$	θ_{f1}	θ_{f2}	θ_s
10	0	0	0.71	81	69	63	0	0	0
30	0.15	0.15	0.74	78	67	57	0	16	26.8
57	0.53	0.53	0.74	75	67	55	0	33	42.5
100	0.85	0.94	0.74	78	69	54	10	44	53.0
300	1.90	2.17	0.74	88	83	53	23	56	68.6
400	—	2.52	0.74	90	90	—	—	—	72.2
				Measured in angular degrees from the forward stagnation point.			Measured in angular degrees from the rear stagnation point		

at the downstream end of the water sphere with a normalized length (L/d) that is slightly less than that of the rigid sphere, where L is the length of the eddy and $d=2a$. The angular extent of the eddy must be described by two angles, the flow separation angle θ_{f_1} which is measured from the rear stagnation point to the place where the eddy separates at the surface of the water sphere, and the angle θ_{f_2} which is measured from the rear stagnation point to the farthest upstream extension of the eddy. For all Reynolds numbers both angles are noticeably smaller than the separation angle θ_s for the rigid sphere. At $20 \leqslant N_{Re} \leqslant 100$, the eddy, even though present, is not in contact with the liquid sphere surface. At these Reynolds numbers the stress exerted by the weak circulation in the trailing vortex is insufficient to counteract the rearward motion of the vortex in the water sphere so that on the surface itself the flow separation point is moved all the way back to the rear stagnation point and the trailing vortex is forced away from the sphere surface. With increasing

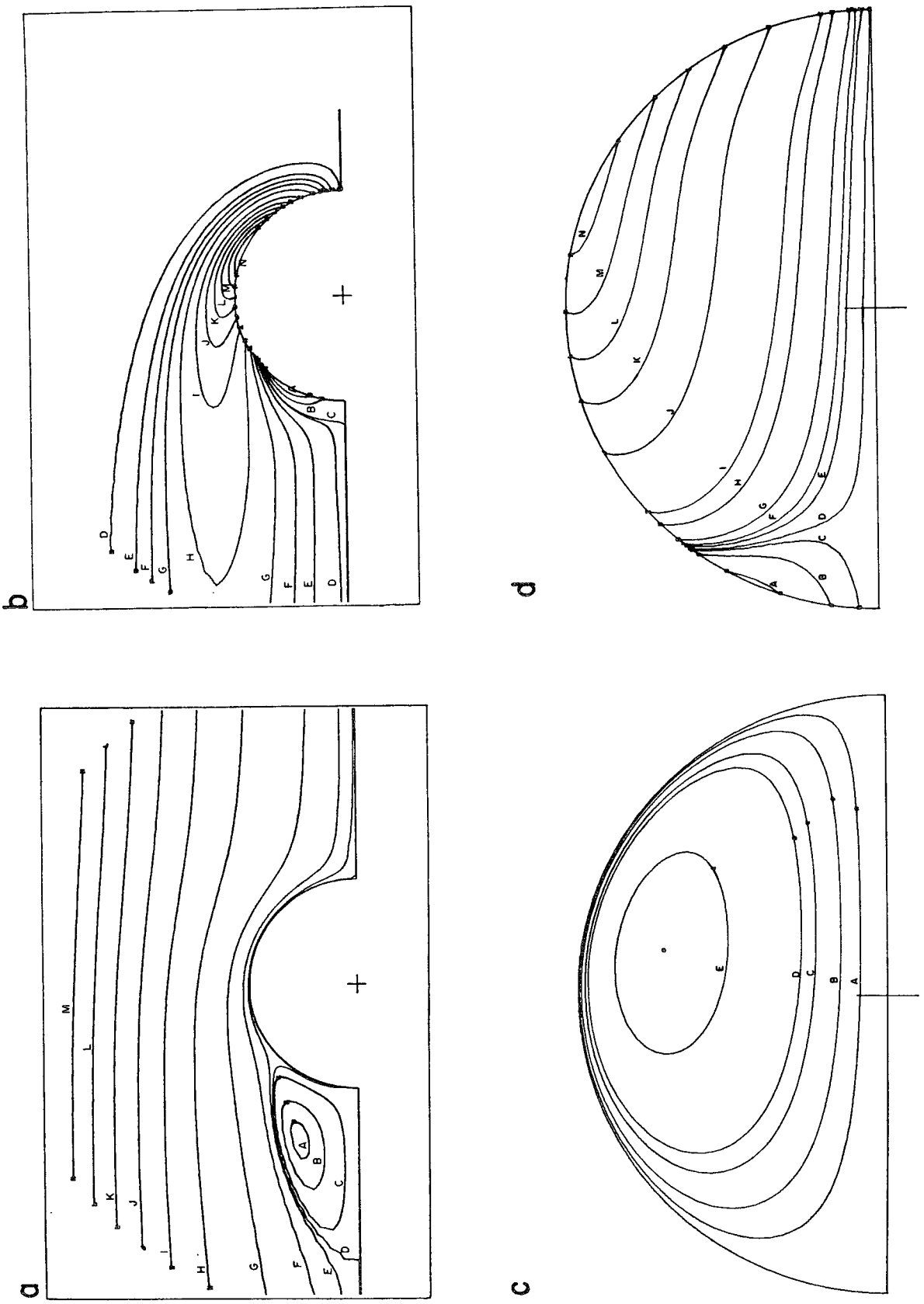

FIG. 5. Same as Fig. 4 except for $N_{Re} = 100$.

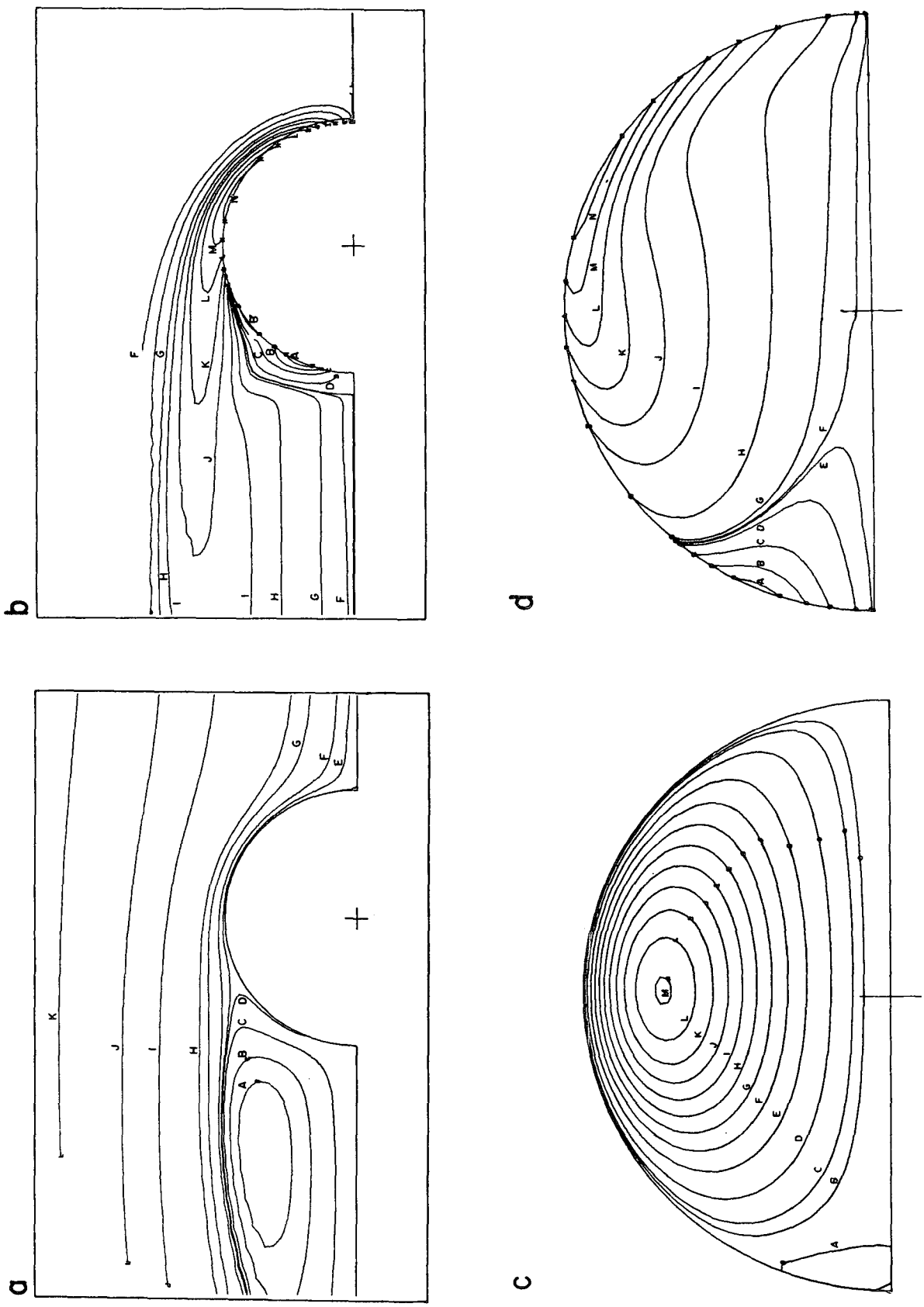

FIG. 6. Same as Fig. 4 except for $N_{Re}=300$.

Reynolds numbers, circulation in the trailing vortex gains strength and the resulting tangential stress is sufficiently large to move the flow separation point upstream so that at $N_{Re}>100$ the trailing vortex is attached to the sphere. At $N_{Re}=300$ the attachment angle is still small but the tangential stress is sufficiently large to cause the creation of a small secondary vortex inside the water sphere with a circulation which is in a sense opposite to that of the main vortex. This phenomenon was first predicted by Hamielec and Johnson (1962). The main vortex in the water sphere is driven by the tangential stress exerted by air flowing downstream over the front half of the sphere. As the Reynolds number increases the maximum tangential stress in the external flow at the surface moves continuously upstream so that $\theta_{\tau_{max}}$ becomes smaller. As a consequence one would expect that the stagnation ring of the primary internal circulation, whose position is given by θ_{st}, would move upstream as well. In reality, however, the stagnation ring of the primary internal vortex moves upstream with increasing Reynolds number for $N_{Re}<57$. At $N_{Re}>57$ the stagnation ring moves back downstream again reaching the position $\theta_{st}=90°$ at $N_{Re}=400$. This behavior can be understood if we realize that the higher the Reynolds number the more efficiently is the vorticity, which penetrates the drop, transported downstream in the drop by means of the internal circulation. Eventually, at a high enough Reynolds number, sufficient vorticity is being advected downstream inside the sphere that, despite the upstream movement of the location of the vorticity production outside the sphere, the primary internal vortex, which tends to establish itself in the region of highest vorticity, moves downstream with the advected vorticity. This vorticity advection is particularly obvious in Fig. 6d. In contrast to the considerable angular movement of the stagnation ring, its radial position is at $N_{Re}=10$ (the one predicted by Hadamard and Rybczynski for low Reynolds numbers), namely, $r'=1/2^{\frac{1}{2}}=0.71$. With increasing Reynolds numbers the primary vortex ring moves slightly outward to $r'=0.74$.

The strength of the primary vortex was chosen to be represented by the velocity $v_i(a,\theta)$ at the surface of the water sphere. The computed velocities are listed in Table 6 as a function of angle and Reynolds number. It is seen from Tables 5 and 6 that the surface velocity maximum moves with increasing Reynolds number first upstream and then downstream in the same manner as the stagnation ring. Thus, with increasing Reynolds number the angle $\theta(v_{i,max})$, which characterizes the position of this maximum, decreases at first from its low Reynolds number value of 90° but then increases again to reach 90° at $N_{Re}=400$.

An interesting and very useful feature of $v_i(a,\theta)/U_\infty$ is brought out by Fig. 7 where a plot is made of $v_i(a,75°)/U_\infty$ vs N_{Re}. The results of the numerical analysis (curve 2a) show that toward high Reynolds numbers $v_i(a,75°)/U_\infty$ approaches the limiting value of 0.042 at $N_{Re}=400$. Toward low Reynolds numbers $v_i(a,75°)/U_\infty$ approaches the limiting value of 0.0086 predicted by Hadamard and Rybczinski. A similar behavior is exhibited by the circulation speed inside an air bubble rising in water (curve 1). At low Reynolds numbers the numerical analysis of LeClair and Hamielec (1971) gives $v_i(a,90°)/U_\infty$ values for a gas bubble in water which approach the value 0.50 predicted by Hadamard and Rybczinski and at higher Reynolds numbers [the value 1.50 was predicted by Boussinesq (1905)]. A limiting value toward high Reynolds numbers is also reached by $v_0(\delta,75°)/U_\infty$ of the flow outside of a circulating water sphere in air (curve 3). These numerical results are in sharp contrast to the results derived from the boundary layer approach (curve 2b). Using Eq. (20) one predicts that $v_i(a,75°)/U_\infty$ would increase indefinitely as N_{Re} increases, a result which is untenable. The fact that $v_i(a,75°)/U_\infty$ derived from the numerical results approaches a constant value at $N_{Re}\approx 400$ permits computing $v_i(a,75°)$ from known values of U_∞ even for $N_{Re}>400$. Such a computation was made using for U_∞ the terminal fall velocities of deformable water drops in air as determined experimentally by Beard and Pruppacher and Gunn and Kinzer, and using the terminal fall velocities of rigid water spheres in air as derived from experimental drag data given by Pruppacher *et al.* The results are graphically displayed in Fig. 1 as curves 3a and 3b.

TABLE 6. Variation of the nondimensionalized surface velocity of the circulating water sphere with angle and Reynolds number, computed in the numerical analysis.

θ (deg)	N_{Re} 10	30	57	100	300
0	0.0	0.0	0.0	0.0	0.0
6	0.0022	0.0028	0.0038	0.0048	0.0048
12	0.0044	0.0056	0.0074	0.0096	0.0096
18	0.0065	0.0083	0.0109	0.0142	0.0142
24	0.0084	0.0108	0.0141	0.0186	0.0186
30	0.0102	0.0130	0.0171	0.0228	0.0227
36	0.0118	0.0150	0.0197	0.0265	0.0265
42	0.0131	0.0167	0.0220	0.0299	0.0300
48	0.0142	0.0181	0.0238	0.0327	0.0331
54	0.0149	0.0191	0.0251	0.0349	0.0359
60	0.0155	0.0197	0.0260	0.0363	0.0383
66	0.0157	0.0200	0.0264	0.0370	0.0403
72	0.0157	0.0199	0.0263	0.0368	0.0418
78	0.0154	0.0194	0.0257	0.0357	0.0428
84	0.0150	0.0185	0.0247	0.0338	0.0431
90	0.0143	0.0174	0.0232	0.0311	0.0423
96	0.0135	0.0161	0.0213	0.0279	0.0403
102	0.0126	0.0146	0.0191	0.0242	0.0370
108	0.0115	0.0130	0.0167	0.0204	0.0324
114	0.0104	0.0113	0.0142	0.0167	0.0271
120	0.0093	0.0096	0.0117	0.0133	0.0217
126	0.0082	0.0081	0.0094	0.0102	0.0167
132	0.0071	0.0066	0.0074	0.0077	0.0126
138	0.0061	0.0053	0.0056	0.0055	0.0092
144	0.0050	0.0041	0.0041	0.0037	0.0060
150	0.0041	0.0031	0.0029	0.0023	0.0030
156	0.0032	0.0023	0.0019	0.0012	0.0004
162	0.0023	0.0016	0.0011	0.0005	−0.0012
168	0.0015	0.0010	0.0006	0.0001	−0.0018
174	0.0008	0.0005	0.0002	−0.0000	−0.0012
180	0.0	0.0	0.0	0.0	0.0

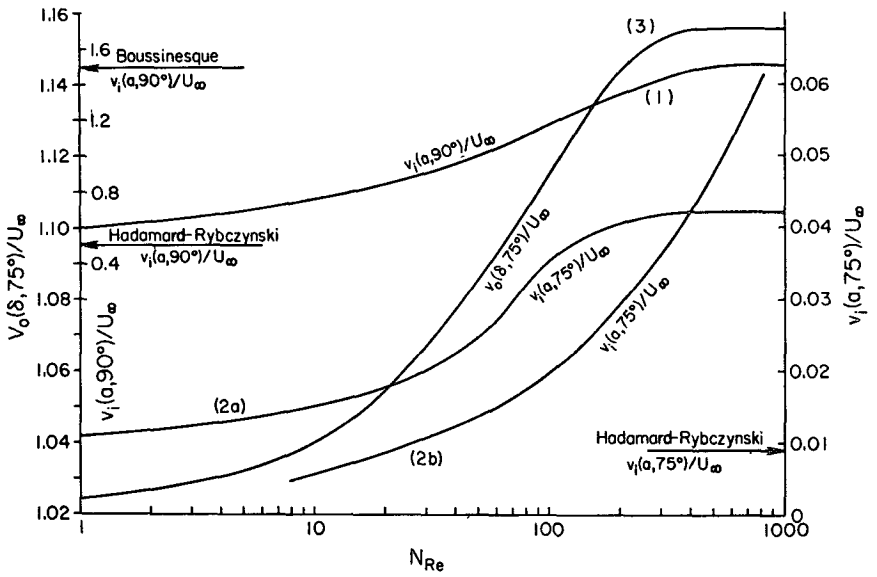

FIG. 7. Variation of the tangential velocity with Reynolds numbers: curve 1, velocity at the surface of an air bubble rising in water (numerical approach); curve 2a, velocity at the surface of a circulating water sphere in air (numerical approach); curve 2b, velocity at the surface of a circulating water sphere in air (boundary layer approach); and curve 3, velocity at the edge of the boundary layer outside a circulating water sphere in air (numerical approach). The outer ordinate to the left belongs to curve 3, the inner ordinate to the left to curve 1, and the ordinate to the right to curves 2a and 2b.

4. Conclusions

The results of the different analyses presented above are compared in Fig. 1. The results of the inviscid flow analysis have not been included in Fig. 1 since it can readily be deduced from Eq. (10) that this analysis strongly overestimates the internal velocities over the whole range of drop sizes. This result is expected in that it is physically untenable to disregard the viscous nature of the flow inside and outside the drop. In contrast, the low Reynolds number approach proposed by Hadamard and Rybczinski strongly underestimates the internal circulation strength over the whole range of drop sizes; this result is also expected since it is known from the work of LeClair *et al.* and Pruppacher *et al.* that the Stokes drag underestimates the actual drag and thus underestimates the stress on a sphere at all Reynolds numbers, particularly when $N_{Re}>0.1$. The boundary-layer approach, in combination with Tomotika's results and a velocity distribution outside the sphere given by numerical methods, seems to give results which are in fair agreement with experiment for $a_0<500\,\mu$. For larger drop sizes, boundary layer theory drastically overestimates the true strength of the internal circulation. The results of the numerical analysis agree well with the experimental results for $a_0<500\,\mu$. For $a_0>500\,\mu$ this approach also overestimates the strength of the internal circulation, but it does predict the correct trend, if the observed terminal velocities of deformable water drops in air are used for U_∞. It is not straightforward to explain why the numerical analysis correctly predicts the strength of the internal circulation in drops with $a_0<500\,\mu$ but fails for drops $>500\,\mu$ in radius. However, three reasons shall be cited. First, the numerical analysis, as do the other approaches, assumes that the water drop has a spherical shape. It was shown by Pruppacher and Beard and by Pruppacher and Pitter that this assumption can be approximately justified if the drops have radii $<500\,\mu$. Larger drops are deformed into oblate spheroids which, with increasing size, develop a flattened base and subsequently a concave depression. One could therefore conjecture that the area over which the tangential stress, exerted by the air, acts on the drop becomes rapidly smaller with increasing drop deformation. Thus, increased drop deformation results in decreased internal circulation. This argument is, however, not very compelling since the drop deformation is not really that great for the drop sizes over which the results from experiment and theory diverge. Second, it has been shown by many workers that drops with $a_0>500\,\mu$ have a tendency to oscillate. The present wind tunnel experiments as well as the earlier experiments made by Pruppacher and Beard clearly demonstrated that such oscillations tend to disrupt organized internal circulation. This disruption leads to a periodic break-up and reformation of the internal circulation such that the internal circulation velocity may, for a fraction of a second, drop almost to zero and shortly after reach a maximum in order to decay again and so on. Therefore, in Fig. 1 we recorded our measurements by indicating the maximum velocity with an arrow pointing toward zero velocity. Third, the external flow in the rear of a falling drop becomes increasingly im-

portant in determining the internal flow pattern as the Reynolds number of the falling drop increases. In Fig. 6c the internal return circulation induced by the external standing eddy at the rear of the drop is clearly seen. At Reynolds numbers $\gtrsim 400$ shedding of vortices from the rear of the falling drop takes place. Since this feature is not taken into account in the axisymmetric flow model of the numerical analysis, it is clear that the effect of the external flow in the rear of the drop on the internal flow is not accurately taken into account by extrapolating the numerical computation to Reynolds numbers >400, in the manner mentioned above.

While the present experimental technique involving streak photography made it possible to make quantitative determinations of the strength of the internal circulation in water drops, the technique was not suitable for a similar evaluation of the position of the stagnation ring. This was due to the fact that for determining the internal velocity a very low concentration of tracer particles had to be used. Nevertheless, the available motion picture data allowed the conclusion that $70 \lesssim \theta_{st} \lesssim 80°$ for drops with $306 \leqslant a_0 \leqslant 411\,\mu$ ($100 \leqslant N_{\mathrm{Re}} \leqslant 180$), and that $\theta_{st} \approx 90°$ for drops with $a_0 > 1$ mm ($N_{\mathrm{Re}} > 866$), in fair agreement with the numerical predictions. This is illustrated by Fig. 2 where an effort is made to visualize the internal circulation in a drop with a $a_0 = 315\,\mu$ ($N_{\mathrm{Re}} = 105$) by using a larger number of particles; the resulting contrast was such that the instantaneous flow pattern could be seen after reproduction.

Acknowledgments. Two of the authors (B. P. L. and A. E. H.) would like to express their gratitude to the National Research Council of Canada, and the other two (H. R. P. and W. D. H.) are greatly indebted to the National Science Foundation (GA-18531) for supporting the research reported in this paper.

APPENDIX A

The Effect of Internal Circulation on Drop Shape

Based on an analysis of the forces acting on a water drop which falls at terminal velocity in air, Pruppacher and Pitter recently presented a method for computing the equilibrium shape of a drop. Foremost, this method requires a knowledge of the surface pressure distribution around the drop. The theoretical expression for the pressure at the surface of a liquid circulating sphere is given by Eq. (28). A comparison of this equation with that for the pressure distribution around a rigid sphere, given by LeClair (1970) as

$$k(a,\theta) = k(a,\theta=0) + \frac{4}{N_{\mathrm{Re}}} \int_0^{\theta} \left(\frac{\partial \zeta}{\partial r} + \zeta \right)_{r=1} d\theta, \quad \text{(A1)}$$

shows that the effect of a non-zero tangential velocity at the surface of a liquid sphere is to reduce the pressure at all points of the sphere surface; in other words, the pressure becomes less positive near the forward stagnation point where the pressure is positive, while at the sphere surface near the equator and on the downstream hemisphere of the sphere where the pressure is negative the pressure becomes more negative than at corresponding locations on a rigid sphere. This result is illustrated by Table 7 for the case that $N_{\mathrm{Re}} = 300$. It would be tempting to derive from this result some conclusions as to the effect of internal circulation on drop shape by substituting the present pressure distribution around a liquid circulating sphere into the force balance equation of Pruppacher and Pitter and determine the drop curvature as a function of θ and thus the drop deformation. However, before such a computation can be made one has to realize that in the liquid case external as well as internal pressures change upon onset of circulation. Since both the external and internal pressure force enters the force balance equation for deforming drop shape, and since at present no quantitative computations are available on the internal pressure distribution of a liquid circulating sphere, it does not appear that one can argue convincingly regarding the type of distortion the internal circulation might produce in a drop, although Foote (1969), using the Bernoulli equation, attempted to argue in favor of a decrease in curvature in the vicinity of the drop waist. However, it is interesting to note that the results of Pruppacher and Pitter indicate that the deformation of water drops in air, computed from the pressure distribution around a rigid sphere, are in good agreement with the deformation measured on drops in a wind tunnel, as long as $a_0 < 2.5$ mm. This suggests that internal circulation plays a negligible role in affecting the drop shape.

TABLE 7. Comparison between the pressure at the surface of a circulating and a rigid water sphere, computed in the numerical analysis, $N_{\mathrm{Re}} = 300$.

θ (deg)	$k(a,\theta)$ Rigid sphere	$k(a,\theta)$ Liquid circulating sphere	Δk
0	+1.037	+1.036	−0.001
36	+0.320	+0.310	−0.010
84	−0.596	−0.630	−0.034
96	−0.499	−0.528	−0.029
120	−0.293	−0.304	−0.011
168	−0.163	−0.179	−0.016

APPENDIX B

The Effect of Internal Circulation on Drag

Assuming very low Reynolds numbers, Stokes flow outside a liquid circulating sphere, and Hadamard-Rybczinski flow inside the sphere, the drag on the sphere is given by (Happel and Brenner, 1965)

$$D = 6\pi a \eta_0 U_\infty \left(\frac{1+\frac{2}{3}\sigma}{1+\sigma} \right). \quad \text{(B1)}$$

TABLE 8. Comparison between the drag coefficients of a circulating and a rigid water sphere, computed in the numerical analysis.

N_{Re}	C_{DF} Rigid	C_{DF} Liquid	C_{DP} Rigid	C_{DP} Liquid	C_D Rigid	C_D Liquid
10	2.77	2.71	1.52	1.51	4.29	4.23
30	1.30	1.29	0.81	0.81	2.11	2.10
57	0.88*	0.88	0.63*	0.63	1.51*	1.51
100	0.59	0.59	0.51	0.49	1.10	1.08
300	0.28	0.29	0.35	0.34	0.63	0.63

* Interpolated.

For $\mu_0=\mu_{air}\ll\mu_i=\mu_{water}$

$$D\approx 6\pi a\eta_0 U_\infty = D_{Stokes}. \tag{B2}$$

From this low Reynolds number analysis one would suspect that there is little difference between the drag on a circulating water sphere in air and the drag on a rigid sphere. This result was verified, indeed, in the present numerical analysis. According to LeClair (1970), the drag coefficients can be expressed by

$$C_{DP}=\int_0^\pi k(a,\theta)\sin(2\theta)d\theta, \tag{B3}$$

$$C_{DF}=\frac{8}{N_{Re}}\int_0^\pi\left[\left(\frac{\partial v}{\partial r}-v\right)\sin\theta-2\frac{\partial u}{\partial r}\cos\theta\right]\sin\theta d\theta, \tag{B4}$$

where u is the radial velocity, v the tangential velocity of the flow field, and $C_D=C_{DP}+C_{DF}$. Eqs. (B3) and (B4) were numerically evaluated for water spheres in air. The results are listed in Table 8 where comparison is made with the drag coefficients for a rigid sphere. As expected from the low Reynolds number analysis, the difference between the drag for a circulating water sphere and a rigid sphere is very small indeed, the drag for a liquid circulating sphere being smaller than the drag on a rigid sphere by less than about 1%. Previous conjectures (Foote and du Toit, 1969; McDonald, 1960) that the internal circulation affects the drag by more than this value are hardly justifiable since they were based on older drag measurements on water drops and rigid spheres which cannot be considered accurate enough. On the other hand, a comparison between the wind tunnel measurements of Beard and Pruppacher (1969) on water drops falling at terminal velocity in air and the most recent drag measurements on rigid spheres (Beard and Pruppacher) showed that there is no difference between the drag on a water drop and that on a rigid sphere of the same Reynolds number, as long as the drop can be assumed to have spherical shape. Thus, the present numerical results agree well with those of Beard and Pruppacher.

REFERENCES

Beard, K. V., and H. R. Pruppacher, 1969: A determination of the terminal velocity and drag of small water drops by means of a wind tunnel. *J. Atmos. Sci.*, **26**, 1066–1072.

Blanchard, D. C., 1949: Experiments with water drops and the interaction between them at terminal velocity in air. Project Cirrus, Occasional Rept. No. 17, General Electric Research Laboratory, Schenectady, N. Y., 29 pp.

Boussinesq, M. J., 1905: Calcul du pouvoir refroidissant des courants fluides. *J. Math. Pure Appl.*, **11**, 285–332.

Foote, G. B., 1969: On the internal circulation and shape of large raindrops. *J. Atmos. Sci.*, **26**, 179–181.

——, and P. S. du Toit, 1969: Terminal velocity of rain drops aloft. *J. Appl. Meteor.* **8**, 249–253.

Garner, F. H., and J. J. Lane, 1959: Mass transfer to drops of liquid suspended in a gas stream. *Trans. Inst. Chem. Eng., London*, **37**, 167–172.

Gunn, R., and G. D. Kinzer, 1949: The terminal velocity of fall for water drops in stagnant air. *J. Meteor.*, **6**, 243–248.

Hadamard, J., 1911: Mouvement permanent lent d'une sphere liquid et visqueuse dans un liquid visqueux. *Compt. Rend.*, **152**, 1735–1738.

Hamielec, A. E., and A. I. Johnson, 1962: Viscous flow around fluid spheres at intermediate Reynolds numbers. *Can. J. Chem. Eng.*, **40**, 41–45.

Happel, J., and H. Brenner, 1965: *Low Reynolds Number Hydrodynamics*. Englewood Cliffs, N. J., Prentice-Hall, 553 pp.

Horton, T. J., J. R. Fritsch and R. C. Kintner, 1965: Experimental determination of circulating velocities inside drops. *Can. J. Chem. Eng.*, **43**, 143–146.

Kintner, R. C., T. J. Horton, R. E. Graumann and S. Auberhar, 1961: Photography in bubble and drop research. *Can. J. Chem. Eng.*, **39**, 235–241.

Le Clair, B. P., 1970: Viscous flow in multiparticle systems at intermediate Reynolds numbers. Ph.D. thesis, Dept. of Chemical Engineering, McMaster University, Hamilton, Canada.

——, and A. E. Hamielec, 1971: Viscous flow through particle assemblages at intermediate Reynolds numbers—A cell model for transport in bubble swarms. *Can. J. Chem. Eng.*, **49**, 713–720.

——, ——, and H. R. Pruppacher, 1970: A numerical study of the drag on a sphere at low and intermediate Reynolds numbers. *J. Atmos. Sci.*, **27**, 308–315.

Lenard, P., 1904: Ueber Regen. *Meteor. Z.*, **21**, 249–260.

McDonald, J. E., 1954: The shape and aerodynamics of large raindrops. *J. Meteor.*, **11**, 478–494.

——, 1960: A note on the aerodynamic effects of Internal circulation in small rain drops. *J. Meteor.*, **17**, 474–494.

Milne-Thomson, L. M., 1967: *Theoretical Hydrodynamics*, 5th ed. New York, MacMillan, 743 pp.

Pruppacher, H. R., and K. V. Beard, 1970: A wind tunnel investigation of the internal circulation and shape of water drops falling at terminal velocity in air. *Quart. J. Roy. Meteor. Soc.*, **96**, 247–256.

——, LeClair, B. P. and A. E. Hamielec, 1970: Some relations between the drag and flow pattern of viscous flow past a sphere and a cylinder at low and intermediate Reynolds numbers. *J. Fluid Mech.*, **44**, 781–790.

——, and R. Pitter, 1971: A semi-empirical determination of the shape of cloud and rain drops. *J. Atmos. Sci.*, **28**, 86–94.

Rybczinski, W., 1911: *Bull. Acad. Caracovie, Ser A.*, p. 40 (referred to in Lamb, H., 1932: *Hydrodynamics*, Cambridge University Press, 738 pp.).

Tomotika, S., 1937: The laminar boundary layer on the surface of a sphere in a uniform stream. Great Britain, Aero. Res. Comm., Rept. and Memo. No. 1678, 86–99.